

AD-A161 770

ASYMPTOTIC ANALYSIS OF A MODE I CRACK PROPAGATING
STEADILY IN A DEFORMATION THEORY MATERIAL(U) HARVARD
UNIV CAMBRIDGE MA DIV OF APPLIED SCIENCES

141

UNCLASSIFIED

P P CASTANEDA SEP 85 MCCH-71

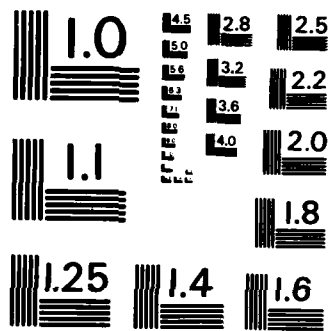
F/G 20/11

NL

END

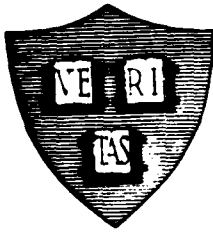
이성민

DTIC



MICROCOPY RESOLUTION TEST CHART
NATIONAL BUREAU OF STANDARDS - 1963 - A

(12)



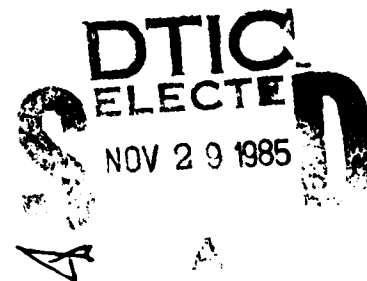
MECH-71

AD-A161 770

ASYMPTOTIC ANALYSIS OF A MODE I CRACK PROPAGATING
STEADILY IN A DEFORMATION THEORY MATERIAL

P. Ponte Castañeda

DTIC FILE COPY



Division of Applied Sciences
HARVARD UNIVERSITY
Cambridge, Massachusetts 02138

September 1985

This document has been approved
for release and sale; its
distribution is unlimited.

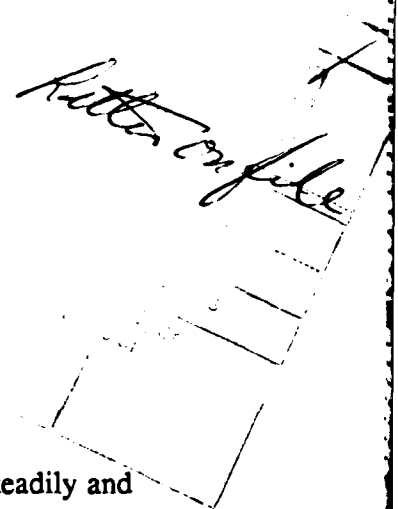
85 10 28 088

ASYMPTOTIC ANALYSIS OF A MODE I CRACK PROPAGATING STEADILY IN A DEFORMATION THEORY MATERIAL

P. Ponte Castañeda

Division of Applied Sciences
Harvard University
Cambridge, Massachusetts 02138

Letter on file



A-1

Abstract

The asymptotic stress and deformation fields of a crack propagating steadily and quasi-statically into an elastic-plastic material are presented. The material is characterised by J_2 deformation theory, suitably modified to account for unloading and reloading, together with linear strain-hardening. The cases of plane-strain and plane-stress mode I are considered. The associated governing equations are integrated analytically, and the boundary conditions lead to algebraic nonlinear equations which are solved numerically. Results are given for the strength of the singularity, and for the distribution of stress in the plastic loading, elastic unloading and plastic reloading regions, as functions of the strain-hardening parameter.

1. Introduction

Knowledge of the stress and deformation fields near the tip of an advancing crack is central to the continued development of engineering fracture mechanics, and important advances have been made in recent years. Under the assumption of quasi-static growth and small-strain ideal elasto-plasticity, rigorous asymptotic solutions have been found in anti-plane strain by Chitaley and McClintock (1971); in plane strain by Slepyan (1974), Gao

(1980), Rice *et al.* (1980) and Drugan *et al.* (1982); and in plane-stress mode II by Ponte (1985a). In addition, a general discussion of the subject is found in Rice (1982).

The corresponding work for hardening elastic-plastic solids is at a less developed stage. Slepyan (1973) provided the near-tip fields of a mode III crack propagating steadily in a linear-hardening J_2 -deformation theory material. Also for linear-hardening materials, Amazigo and Hutchinson (1977) produced steady-state asymptotic solutions using J_2 -flow theory for modes I (plane strain and plane stress) and III. These solutions, however, neglected the possibility of reverse plastic flow on the crack flanks which is known to occur in the elastic perfectly-plastic solutions mentioned above. Zhang *et al.* (1983) included reloading (as well as a Bauschinger effect) in their solution of the plane-strain mode I problem. More recently, Ponte (1985b) provided a complete set of solutions including reloading for modes I (plane strain and plane stress), II (plane strain and plane stress) and III.

Further work on the hardening elastic-plastic steadily moving crack include publications by Lo and Pierce (1981) who considered a mode III crack moving in a linear-hardening corner theory material, and Gao *et al.* (1983) who investigated a mode III crack propagating in a power-hardening J_2 -flow theory material.

Even though deformation theory is unreliable for non-proportional loading histories such as that which a near-tip particle experiences as it moves past a crack tip, it is found by comparing the solutions of Slepyan (1973), and Amazigo and Hutchinson (1977) for the mode III case that the deformation theory solution presents the same general features as the flow theory solution. In fact, some of the detailed results such as the dependence of the strength of the singularity on the hardening parameter are in remarkably close agreement. On the other hand, for a linear-hardening material, deformation theory suitably modified to account for unloading and reloading yields an analytically much simpler set-up than flow theory.

In this work we propose to solve the plane-stress and plane-strain mode I asymptotic problems using J_2 deformation theory with linear strain-hardening, and to compare the results to the corresponding flow theory results. We will make use of concise complex-variable formulations that will yield straightforward analytical solutions for the near-tip fields.

2. Formulation

With reference to Figure 2.1, let x_i ($i = 1,2,3$) be a Cartesian coordinate system of fixed orientation travelling with the crack tip such that the x_3 axis coincides with the straight crack front. Also let e_i be the unit vector corresponding to the x_i direction. Similarly, let r, θ be polar coordinates corresponding to x_α ($\alpha = 1,2$), and e_r, e_θ be the corresponding unit vectors. The crack tip moves with velocity $V = Ve_1$ with respect to the stationary coordinate system X_i . In our steady-state analysis the crack tip speed V is constant so that the material derivative is given by

$$(\)' = -V(\)_{,1} \quad (2.1)$$

For mode I loading of an isotropic material with the given geometry we have that the only non-zero components of the stress tensor are $\sigma_{\alpha\beta}$ ($\alpha, \beta = 1,2$) (and σ_{33} for plane strain). Then, neglecting inertia, the equilibrium equations are

$$\sigma_{\alpha\beta,\alpha} = 0 \quad (2.2)$$

The only non-zero components of the strain tensor are $\epsilon_{\alpha\beta}$ (and ϵ_{33} for plane stress). The equations of compatibility are

$$e_{\alpha\beta} e_{\lambda\mu} \epsilon_{\alpha\lambda,\beta\mu} = 0 \quad (2.3)$$

where $e_{\alpha\beta}$ is the two dimensional permutation symbol ($e_{11} = e_{22} = 0, e_{12} = -e_{21} = 1$).

The constitutive relations are

$$\epsilon_{ij} = \epsilon_{ij}^{el} + \epsilon_{ij}^{pl} \quad (2.4)$$

where the components of the elastic strain tensor are given by

$$\epsilon_{ij}^{el} = (1/E) [(1+\nu) \sigma_{ij} - \nu \sigma_{kk} \delta_{ij}] \quad (2.5)$$

and the plastic strain is given by a deformation theory of plasticity modified to account for unloading and reloading. From previous work we expect to have three different types of sectors asymptotically into the crack tip. As depicted in Figure 2.2, we expect to have a plastic loading sector ahead of the crack ($0 < \theta < \theta_1$), followed by an elastic unloading sector ($\theta_1 < \theta < \theta_2$), followed, in some cases, by a plastic reloading sector ($\theta_2 < \theta < \pi$).

Thus when the material particle P is loading ahead of the crack, the components of its plastic strain tensor are given by

$$\epsilon_{ij}^{pl} = (3/2) (1/E_s - 1/E) s_{ij} \quad (2.6)$$

where s_{ij} are the components of the stress-deviator tensor, and $E_s = E_s(\sigma_e)$ is the secant modulus, which is a function of the effective stress $\sigma_e = [(3/2)s_{ij}s_{ij}]^{1/2}$. For a bilinear material with the uniaxial stress-strain relation depicted in Figure 2.3 equation (2.6) reduces to

$$\epsilon_{ij}^{pl} = (3/2) (1/E) (1/\alpha - 1) (1 - \sigma_o/\sigma_e) s_{ij} \quad (2.7)$$

where σ_o is the yield stress in tension, and α is the ratio of the tangent modulus, E_t , to the elastic modulus, E .

Note that for $|\sigma_o/\sigma_e| \ll 1$, equation (2.7) simplifies to

$$\epsilon_{ij}^{pl} = (3/2) (1/E) (1/\alpha - 1) s_{ij} \quad (2.8)$$

Observing that for small non-dimensional r , we expect $\sigma_e/\sigma_o = O(r^s)$ (where $-1/2 \leq s < 0$ for $0 < \alpha \leq 1$), it follows that, sufficiently close to the crack tip ($0 < r \ll e^{-1/|s|}$), and provided that $\sigma_e \neq 0$, equation (2.8) is a valid approximation to (2.7). Note that the approximation breaks down as $\alpha \rightarrow 0$. We conclude that for $0 < \alpha \leq 1$

$$\epsilon_{ij} = (1/E^*) [(1+\nu^*) \sigma_{ij} - \nu^* \sigma_{kk} \delta_{ij}] \quad (2.9)$$

where $E^* = \alpha E$ and $\nu^* = \alpha(2\nu-1)/2 + 1/2$.

When the particle unloads elastically at location 1 in Figure 2.2, its plastic strain is assumed to be continuous across the boundary. As it moves through the elastic sector, its

plastic strain remains constant. Thus the plastic strain in the elastic unloading sector is specified by

$$\epsilon_{ij}^{pl} = [\epsilon_{ij}^{pl}]^1 \quad (2.10)$$

Note that $[\epsilon_{ij}^{pl}]^1$ is a function of x_2 only, and is evaluated for a given particle by letting $x_1 = \bar{x}_2/\tan \theta_1$ in (2.8).

When the particle reloads plastically at location 2 in Figure 2.2, its plastic strain is again assumed to be continuous across the boundary, and hence is the same as the plastic strain that it had just before it unloaded. Thus the plastic strain in the plastic reloading sector is given by

$$\epsilon_{ij}^{pl} = (3/2) (1/E) (1/\alpha-1) s_{ij} - [\epsilon_{ij}^{pl}]^2 + [\epsilon_{ij}^{pl}]^1 \quad (2.11)$$

where $[\epsilon_{ij}^{pl}]^2$ is evaluated for a given particle by letting $x_1 = \bar{x}_2/\tan \theta_2$ in (2.8). Note that any further unloading/reloading can be modeled in a similar manner.

Equations (2.2), (2.3) and (2.4) together with (2.5) and either (2.8), (2.10) or (2.11) (depending on whether loading, unloading or reloading occurs, respectively) are the governing equations in each sector.

We solve these equations in any given sector by first introducing a stress function f to satisfy equilibrium so that

$$\sigma_{\alpha\beta} = e_{\alpha\lambda} e_{\beta\mu} f_{,\lambda\mu} \quad (2.12)$$

Next note that in the plastic loading sector we effectively have an elastic problem with modified elastic constants E^* and ν^* , and compatibility yields

$$\nabla^4 f = 0 \quad (2.13)$$

where we have used the fact that for plane stress $\sigma_{33} = 0$, and for plane strain $\epsilon_{33} = 0$ (which implies $\sigma_{33} = \nu^* \sigma_{\alpha\alpha}$). The solution of (2.13) can be expressed as

$$f = \text{Re}\{ \bar{z} \phi(z) + \chi(z) \} \quad (2.14)$$

where ϕ and χ are analytic functions of $z = re^{i\theta}$ in the sector. Since we are interested in asymptotic results we will assume the following forms for ϕ and χ

$$\phi(z) = az^s \quad \psi(z) = \chi'(z) = bz^s \quad (2.15)$$

where a and b are undetermined complex constants. The stress components $\sigma_{\alpha\beta}$ can then be found in terms of a , b and s by means of the Muskhelishvili complex variable relations given in Appendix A.

In the elastic unloading sector compatibility and either the plane stress or plane strain condition lead to

$$(1-\nu^2) \nabla^4 f = -E \{ [\epsilon_{11}^{pl}]^1 + \nu [\epsilon_{33}^{pl}]^1 \}_{,22} \quad (2.16)$$

where $\nu = 0$ for plane stress, or $\nu = \nu$ for plane strain. The solution to this P.D.E. can be written as

$$f = f^h + f^{pa} \quad (2.17)$$

where f^{pa} is any particular solution of the P.D.E, and the homogeneous solution f^h is given by an expression similar to (2.14) with new functions ϕ and χ (analytic in the sector) which are of the form of (2.15) but with different complex coefficients c and d . It follows that we can write

$$\sigma_{\alpha\beta} = \sigma_{\alpha\beta}^h + \sigma_{\alpha\beta}^{pa} \quad (2.18)$$

where the $\sigma_{\alpha\beta}^h$ can be expressed through f^h in terms of the new ϕ and ψ , and f^{pa} can be chosen such that

$$\sigma_{11}^{pa} = -[E/(1-\nu^2)] \{ [\epsilon_{11}^{pl}]^1 + \nu [\epsilon_{33}^{pl}]^1 \} \quad (2.19)$$

$$\sigma_{12}^{pa} = \sigma_{22}^{pa} = 0$$

In the plastic reloading sector compatibility and either the plane stress or plane strain condition lead to

$$[1 - (\nu^*)^2] \nabla^4 f = E^* \{ [\epsilon_{11}^{pl}]^2 - [\epsilon_{11}^{pl}]^1 + \nu^* ([\epsilon_{33}^{pl}]^2 - [\epsilon_{33}^{pl}]^1) \}_{,22} \quad (2.20)$$

This equation is of the same form as equation (2.16), and can be solved in the same manner. Equation (2.18) applies with new constants e and f for the functions ϕ and ψ in the expressions for the homogeneous stresses, and equations similar to (2.19) for the particular stresses.

Noting that the inhomogeneous terms in equations (2.16) and (2.20) are functions of x_2 only, it pays to consider the material derivatives of these equations (and also of equation (2.13) for consistency). Thus we find that the same homogeneous equation governs in all three sectors

$$\nabla^4 \mathfrak{S} = 0 \quad (2.21)$$

where $\mathfrak{S} = f^*$ is the stress-rate function. The solution to (2.21) is given by

$$\mathfrak{S} = \text{Re}\{ \bar{z} \Phi(z) + X(z) \} \quad (2.22)$$

where Φ and X are analytic in each sector. For consistency, in the plastic loading sector we let

$$\Phi(z) = Az^{s-1} \quad \Psi(z) = X'(z) = Bz^{s-1} \quad (2.23)$$

where A and B are undetermined complex constants, but are related to a and b through

$$A = -sVa \quad B = -sV(a+b) \quad (2.24)$$

Note that even though it will turn out that it is most convenient to use the stress-rate function coefficients A and B in the formulation of the problem, with this simple conversion we can always go back to our original expressions above to find the stress components. Expressions analogous to (2.23) and (2.24) apply in the elastic unloading and plastic reloading sectors, but with complex coefficients pairs C, D and E, F , respectively.

Later we will need expressions for the traction-rate force F and the velocity vector v in terms of the Muskhelishvili rate functions, and these are also given in Appendix A.

It is clear from the formulation in terms of the stress function that this is a fourth order problem. Given the variable-separable nature of the solution ($z = re^{i\theta}$), we need to impose four boundary conditions in θ . Mode I symmetry requires

$$u_2(r,0) = \sigma_{12}(r,0) = 0 \quad (2.25)$$

and the traction-free condition on the crack faces requires

$$\sigma_{12}(r,\pi) = \sigma_{22}(r,\pi) = 0 \quad (2.26)$$

Note that these four conditions are homogeneous, and lead to an eigenvalue problem for s as a function of α (and v). Thus we expect to determine the stress and

deformation distributions only up to an arbitrary amplitude factor analogous to the stress intensity factor in the elastic problem.

Next we need to connect the solutions in the different sectors through some appropriate continuity conditions. Thus we impose four conditions at each unloading and reloading boundary. Let $[]$ denote the jump in a quantity as θ increases infinitesimally; then the traction components of the stress must be continuous

$$[\sigma_{r\theta}] = [\sigma_{\theta\theta}] = 0 \quad (2.27)$$

and the displacement field must also be continuous

$$[u_r] = [u_\theta] = 0 \quad (2.28)$$

Note that in the previous development we imposed continuity of the plastic strains; this should be viewed as part of the constitutive model, and not as continuity conditions independent of (2.27) and (2.28).

The boundary and continuity conditions described above when expressed in terms of stress functions are fairly cumbersome due to the so-called particular terms. It is then useful to rewrite these conditions in terms of rate quantities. Thus the boundary conditions (2.25) and (2.26) take the form

$$v_2(r,0) = \Sigma_{12}(r,0) = 0 \quad (2.29)$$

$$\Sigma_{12}(r,\pi) = \Sigma_{22}(r,\pi) = 0 \quad (2.30)$$

where $\Sigma = \dot{\sigma}$, and $v = \dot{u}$. The last of these two sets of conditions can be rewritten further in terms of the traction-rate force

$$F_1(r,\pi) = F_2(r,\pi) = 0 \quad (2.31)$$

Given conditions (2.27), (2.28) and the continuity of the plastic strain across each elastic-plastic boundary, it can be shown (Ponte, 1985b) that for a strain-hardening material ($0 < \alpha \leq 1$) the stress tensor must be fully continuous. It then follows from the equilibrium equations that the traction components of the stress-rate tensor must be continuous as well

$$[\Sigma_{r\theta}] = [\Sigma_{\theta\theta}] = 0 \quad (2.32)$$

This in turn implies continuity of the traction-rate force vector

$$[F_1] = [F_2] = 0 \quad (2.33)$$

Similarly, it can be shown (Ponte, 1985b) that under the given assumptions the velocity vector must also be continuous

$$[v_1] = [v_2] = 0 \quad (2.34)$$

Thus conditions (2.33) and (2.34) will be used instead of the more primitive conditions (2.27) and (2.28) to connect the fields in the different sectors.

Finally, we need to characterise the onsets of unloading and reloading. For flow theory, σ_e' is continuous across the unloading boundary, and the unloading angle, θ_1 , is uniquely determined by the condition

$$\sigma_e'(r, \theta_1) = 0 \quad (2.35)$$

For deformation theory, however, σ_e' is not in general continuous. This is due to the fact that the component of the strain-rate tensor D_{rr} ($D = \dot{\epsilon}'$) does not necessarily vanish on the plastic side of the unloading boundary (as is the case for flow theory). Consequently, there may be a discontinuity in Σ_{rr} , and therefore in σ_e' . Hence there is a range of possible unloading conditions with extreme conditions

$$\sigma_e'(r, \theta_1-) = 0 \quad (2.36a)$$

$$\sigma_e'(r, \theta_1+) = 0 \quad (2.36b)$$

Of all the possibilities, condition (2.36a) makes most sense physically since it implies that the effective plastic strain-rate vanishes at unloading. On the other hand, if we think of deformation theory as a model for flow theory any other unloading condition would be just as adequate. Slepyan (1973) preferred condition (2.36b) because it gave the most conservative estimate for the strength of the singularity.

The reloading angle, θ_2 , is determined by the condition that the material particle regain the effective stress level it had when it unloaded

$$\sigma_e(\bar{x}_2/\tan\theta_1, \bar{x}_2) = \sigma_e(\bar{x}_2/\tan\theta_2, \bar{x}_2) \quad (2.37)$$

Note that unlike the boundary and continuity conditions, the unloading and reloading conditions (2.36) and (2.37) must include particular terms since they involve non-rate quantities, and cannot be simplified any further.

Conditions (2.29), (2.31), (2.33), (2.34), (2.36a) and (2.37) are expressed in Appendix B in terms of the eigenvalue (s), the complex coefficients of Φ and Ψ (A, B, C, D, \dots), and the unloading and reloading angles (θ_1 and θ_2) for both the two-region problem (no reloading occurs) and the three-region problem (if reloading occurs). Note that for plane stress these conditions are independent of Poisson's ratio (ν), but not so for plane strain. The solution procedures used to obtain the unknowns $s, \theta_1, \theta_2, A, B, C, D, \dots$ are also sketched in this appendix. Once these are found, the stress distribution in the different sectors is determined using the expressions for the stresses determined previously.

3. Results and Discussion

3.1 *Plane stress*

The results for this case are summarised in Figures 3.1 to 3.5 and in Table 3.1. Figure 3.1 shows plots of the strength of the singularity, s , versus the square root of the hardening parameter, α , for two deformation theory materials satisfying the two extreme unloading conditions given by (2.36a) and (2.36b) in the formulation section, and also for the flow theory material (Ponte, 1985b). It is found, as Slepyan (1973) observed for the mode III problem, that the deformation theory with unloading condition (2.36b) results in a stronger singularity (and smaller angular extent of the plastic zone) than its counterpart with unloading condition (2.36a), and that deformation theory in general produces a stronger singularity than flow theory. It is also seen that $s \sim -\alpha^{1/2}$ for small α .

Table 3.1 presents values of s, θ_1 and θ_2 for several values of α ranging between zero and unity for the two deformation theories, and for flow theory. It is seen that the

singularities agree very well for the deformation and flow theories, especially for large strain-hardening. For the less singular deformation theory material (corresponding to condition (2.36a)) the unloading angle θ_1 increases from the elastic value to a maximum value of 90° as $\alpha \rightarrow 0$. The opposite behaviour is observed for the more singular material, and θ_1 gets progressively smaller as $\alpha \rightarrow 0$. The flow theory material shows an intermediate behaviour: θ_1 first increases as α decreases, and then decreases as $\alpha \rightarrow 0$. Reloading occurs for the less singular deformation theory material at the value of the hardening parameter $\alpha^* = 0.215$, it never occurs for the more singular material, and takes place at $\alpha^* - 0.01$ for the flow theory material. The actual size of the reloading sector is considerable for the less singular deformation theory material (up to 20°), and very small for the flow theory material (less than 0.001°).

Figure 3.2 shows plots of the particle (fixed x_2) effective stress for several values of α , and corresponds to the less singular material. By comparison to the elastic result plasticity introduces two new features: unloading with a discontinuous slope $[\sigma_e'] < 0$, and the production of residual stress on the wake of the crack. These phenomena become more significant for smaller α , and in fact the need for the reloading sector becomes evident for small enough α . We also note that this material has two local minima in the elastic unloading sector, whereas the flow theory material has only one. Finally, note that for very small α the effective stress level in the plastic zones approaches a constant value, thus approximating a flat variation as expected.

Figure 3.3 shows plots similar to Figure 3.2 but correspond to the more singular material. It presents the same general features as the previous material except for the fact that reloading never occurs, and that the behaviour in the elastic unloading zone resembles more closely that of the flow theory material .

Figure 3.4 shows plots of the angular (fixed r) variations of the stresses for large and moderate strain-hardening for the deformation material with unloading condition (2.36a). The stress distributions are close to the corresponding flow theory distributions

for large strain-hardening, but get progressively farther away from the flow theory distributions as $\alpha \rightarrow 0$. The main qualitative differences are the jumps in the slopes of σ_{rr} and $\sigma_{\theta\theta}$, and the fact that all the components of the stress tensor approach $\theta = \pi$ with slopes opposite in sign to their flow theory counterparts. This effect is most noticeable for σ_{rr} which becomes positively unbounded near $\theta = \pi$, whereas it becomes negatively unbounded for flow theory.

Figure 3.5 shows plots of the angular variations of the stresses for large and moderate strain-hardening for the deformation material with unloading condition (2.36b). Similar observations are made about the stress distributions as in Figure 3.4, but it is noted that in this case the stress distributions agree more closely with the flow theory results in the elastic unloading sector.

3.2 Plane strain

As it was pointed out in the formulation section, the results for this case are dependent on Poisson's ratio (ν). Here we chose not to investigate this dependence, and all the results presented in this section are for $\nu = 1/3$. These results are summarised in Figures 3.6 to 3.8, and in Table 3.2.

Figure 3.6 shows plots of s versus $\alpha^{1/2}$ for the deformation theory material with unloading condition (2.36a), and for the flow theory material. (For the deformation theory material with unloading condition (2.36b) no consistent solutions were found even for large strain-hardening). For large strain-hardening the two plots are coincident, but as α becomes smaller the two diverge with the deformation theory material showing the stronger singularity. For very small α , the results are unexpected for both materials: the deformation theory material has a discontinuous s versus α curve, and the flow theory material has a non-vanishing s as $\alpha \rightarrow 0$.

Table 3.2 presents values of s , θ_1 and θ_2 for several values of α for the two materials mentioned above. It also presents the values of θ_3 and θ_4 corresponding to the

beginning and end of an isolated plastic sector appearing inside the original elastic unloading sector of the deformation theory material for small values of α . The deformation theory material is found to reload (on the crack flank) at a higher level of hardening ($\alpha^* = 0.391$) than the flow theory material ($\alpha^* \sim 0.3$). Further, the three-region solution becomes inconsistent for the deformation theory material for $0 < \alpha < \alpha^+$ ($\alpha^+ = 0.057$) due to the fact that the material particle reloads inside the elastic unloading sector, thus requiring a five region solution for $0 < \alpha < \alpha^+$. The transition from the three-region solution to the five-region solution is not smooth because the (discontinuous) unloading constraint produces a redistribution of the stress and deformation fields, and it accounts for the discontinuous s versus α curve. Note that appropriate changes and additions to the formulation presented above are needed to treat the five-region problem, but they are quite messy and are not presented here. The unloading angle θ_1 is seen to increase as $\alpha \rightarrow 0$ for both materials; however, for deformation theory it has a maximum value of 90° , whereas for flow theory it reaches much larger values. This fact might account for the necessity of the extra plastic loading sector for deformation theory as $\alpha \rightarrow 0$. The reloading angle θ_2 is found to be of comparable magnitude for both cases.

Figure 3.7 depicts plots of the particle effective stress for several values of α . Unloading is observed, and reloading on the crack flanks takes place at an intermediate value of α . Note that the unloading sector develops a bump which gets higher as α decreases, and for the critical value of $\alpha = \alpha^+$ the three-region solution gives way to the five-region solution. For very small α , and ignoring the sharp unloading sector, this curve resembles the curve corresponding to the flow theory material.

Figure 3.8 shows plots of the angular variations of the stresses for large and moderate strain-hardening. We observe discontinuities in the slopes of σ_{rr} , σ_{33} , and σ_e at both the unloading and reloading boundaries. By comparison to the stress distributions of the flow theory material we find that the distributions look roughly similar near the crack

faces, but become quite different ahead of the crack as α decreases. Also the deformation theory material does not show as high a level of triaxiality as the flow theory material.

4. Conclusions

For a linear-hardening material, a deformation theory of plasticity, adequately modified to take into account unloading and reloading, yields an approximate closed form solution to the stress and deformation fields near the tip of a steadily propagating crack. Inside a region of size $r = e^{-1/|s|}$, the constitutive relations can be linearised to yield modified linear elasticity problems in the different sectors that can be solved analytically using concise complex-variable methods. The range of validity of the approximation vanishes as the hardening parameter (and therefore the singularity) becomes smaller.

For large strain-hardening, the functional dependence of the singularity, s , on the hardening parameter, α , for deformation theory is very close to that for flow theory in both plane stress and plane strain. Remarkably, the s versus α curves for deformation and flow theory remain close for intermediate and small strain-hardening for the plane stress case (and the anti-plane shear case as pointed out by Amazigo and Hutchinson, 1977), but not for the plane strain case where unexpected results are obtained for both theories. In general, however, deformation theory provides a stronger singularity than flow theory in all cases studied (including mode III).

As expected, for large strain-hardening the angular variations of the stresses are similar for both theories, but they become quite different as the hardening becomes smaller. Thus the behaviour of the sizes of the plastic and elastic sectors as measured by θ_1 and θ_2 are also fairly different for both theories as $\alpha \rightarrow 0$.

While for flow theory unloading is uniquely defined by the condition $\sigma_e'(r, \theta_1) = 0$, for deformation theory we must admit a discontinuity in σ_e' at unloading boundaries, and

there is a range of possible unloading conditions between the two extreme conditions $\sigma_e'(r, \theta_1-) = 0$ and $\sigma_e'(r, \theta_1+) = 0$. It was found that the first condition leads to a plastic loading zone ahead of the crack of larger angular extent than that of the second, and also to a weaker singularity s for a given value of α .

Acknowledgements

This work was supported in part by the Office of Naval Research under Contract N00014-84-K-0510, and by the Division of Applied Sciences, Harvard University. The author is grateful to his advisor B. Budiansky for suggesting this project and for his continued support and encouragement.

References

Amazigo, J.C. and Hutchinson, J.W., "Crack-tip fields in steady crack growth with linear strain-hardening", *J. Mech. Phys. Solids*, **25**, 81-97 (1977).

Chitaley, A.D. and McClintock, F.A., "Elastic-plastic mechanics of steady crack growth under anti-plane shear", *J. Mech. Phys. Solids*, **19**, 147-163 (1971).

Drugan, W.J., Rice J.R. and Sham, T.L., "Asymptotic analysis of growing plane strain tensile cracks in elastic-ideally plastic solids", *J. Mech. Phys. Solids*, **30**, 447-473 (1982).

Gao, Y.-C., "Elastic-plastic field at the tip of a crack growing steadily in perfectly-plastic medium" (in Chinese), *Acta Mechanica Sinica*, **1**, 48-56 (1980).

Gao, Y., Zhang, X. and Hwang, K., "The asymptotic near-tip solution for mode III crack in steady growth in power hardening media", *Int. J. of Fract.*, **21**, 301-317 (1983).

Lo, K. K. and Pierce, D., "Effect of a yield surface vertex on crack-tip fields in Mode III", *J. Mech. Phys. Solids*, **29**, No. 2, 143-152 (1981).

Ponte Castañeda, P., "Asymptotic fields of a perfectly-plastic, plane-stress mode II growing crack", Harvard University, Division of Applied Sciences, Report MECH-70 (1985a)

Ponte Castañeda, P., "Asymptotic fields in steady crack growth with linear strain-hardening", Harvard University, Division of Applied Sciences, Report MECH-69 (1985b)

Rice, J.R., Drugan, W.J. and Sham, T.L., "Elastic-plastic analysis of growing cracks", *Fracture Mechanics: Twelfth Conference*, ASTM-STP 700, 189-219 (1980).

Rice, J.R., "Elastic-plastic crack growth", *Mechanics of Solids: The Rodney Hill 60th Anniversary Volume* (ed. by H.G. Hopkins and M.J. Sewell), Pergamon Press, Oxford, 539-562 (1982)

Slepyan, L.I., "Deformation at the edge of a growing crack", *Mekhanika Tverdogo Tela*, 8, 139-148 (1973).

Slepyan, L.I., "Growing crack during plane deformation of an elastic-plastic body", *Mekhanika Tverdogo Tela*, 9, 57-67 (1974).

Zhang, R., Zhang, X. and Hwang, K., "Near-tip fields for plane strain mode I steady crack growth in linear-hardening material with Bauschinger effect", *Proceedings of ICF International Symposium on Fracture Mechanics* (ed. by K. Hwang, C. Liu, and Q. He), Science Press, Beijing (1983).

Appendix A. Muskhelishvili formulation

Stress

Given the Muskhelishvili functions ϕ and ψ , we can express the stress components corresponding to a homogeneous elastic problem in the following fashion

$$\begin{aligned}\sigma_{11} + \sigma_{22} &= 2[\phi'(z) + \bar{\phi}'(\bar{z})] \\ \sigma_{22} - \sigma_{11} + 2i\sigma_{12} &= 2[\bar{z}\phi''(z) + \psi'(z)]\end{aligned}\tag{A.1}$$

Traction-rate force

The traction-rate force on a boundary C with fixed origin z_0 and variable endpoint z is given by

$$F_1 + iF_2 = \int_C [T_1(s) + iT_2(s)] ds\tag{A.2}$$

where s is the arc length measure along C , $T_\alpha = \sigma_{\alpha\beta}n_\beta$ are the traction stress-rates and n_β define the unit normal to C .

The integral in (A.2) is path-independent, and it can be shown that

$$F_1 + iF_2 = -i(\mathfrak{I}_{,1} + i\mathfrak{I}_{,2})\tag{A.3}$$

Velocity

The velocity expressions depend on the sector

(i) Elastic unloading sector

$$2G(v_1 - iv_2) = \kappa \bar{\Phi}(\bar{z}) - \bar{z}\Phi'(z) - \Psi(z)\tag{A.4a}$$

where $\kappa = (3-\nu)/(1+\nu)$ for plane stress, or $\kappa = 3-4\nu$ for plane strain.

(ii) Plastic loading sectors

$$2G^*(v_1 - iv_2) = \kappa^* \bar{\Phi}(\bar{z}) - \bar{z}\Phi'(z) - \Psi(z)\tag{A.4b}$$

where $\kappa^* = (3-\nu^*)/(1+\nu^*)$ for plane stress, or $\kappa^* = 3-4\nu^*$ for plane strain.

Appendix B. The governing conditions in terms of the unknown constants

Two-region problem ($\alpha^ < \alpha < 1$).*

In this problem we have six unknowns: two real (s and θ_1), and four complex (A , B , C , D) for a total of ten real unknowns. The boundary and continuity conditions reduce to

Symmetry ($\theta = 0$)

$$\bar{A} = A \quad \bar{B} = B \quad (B.1)$$

Vanishing traction-rates ($\theta = \pi$)

$$s \bar{C} + e^{i2s\pi} C + \bar{D} = 0 \quad (B.2)$$

Continuity of traction-rates ($\theta = \theta_1$)

$$se^{i2\theta_1} (\bar{C} - \bar{A}) + e^{i2s\theta_1} (C - A) + (\bar{D} - \bar{B}) = 0 \quad (B.3)$$

Continuity of velocities ($\theta = \theta_1$)

$$(1+v^*) (1+\kappa^*) \bar{A} - \alpha(1+v) (1+\kappa) \bar{C} + \\ (3/2) (\alpha-1) [A + se^{i2(s-1)\theta_1} A + e^{i2s\theta_1} B] = 0 \quad (B.4)$$

The unloading condition ($\sigma_e'(r, \theta_1-) = 0$) implies

$$[(4/3) \gamma^* \cos(s\theta_1) \cos(s-1)\theta_1] A^2 + \\ \cos \theta_1 \{ (s-1) [s+3-4\cos^2\theta_1] A^2 + (s-1) (4\cos^2\theta_1-2) BA + B^2 \} = 0 \quad (B.5)$$

where $\gamma^* = 1$ for plane stress, or $\gamma^* = 1 + 4v^*(v^*-1)$ for plane strain.

Given s , θ_1 and (B.1), equations (B.2) to (B.4) can be viewed as a system of six linear homogeneous equations in the six unknowns A , B , C , \bar{C} , D and \bar{D} . The condition for a non-trivial solution is that the determinant of the system matrix be zero, or

$$[(1-\cos 2\theta_1) \sin 2\theta_1] s^3 + [(1-\delta) (1-\cos 2\theta_1) \sin(2s\theta_1)] s^2 + \\ \{ (1/2)\omega(\delta-\omega) + (1+\omega) [\cos(2s\theta_1)-1] \} \sin(2\theta_1) s + \\ \{ (1-\delta) (1+\omega) [\cos 2s(\theta_1-\pi)-1] \sin(2s\theta_1) - (1/2) \omega (\delta+\omega) \sin(2s\theta_1) + \\ (1/2) \omega \delta \sin[2s(2\theta_1-\pi)] \} = 0 \quad (B.6)$$

where $\omega = (2/3) \alpha (1+v) (1+\kappa) / (1-\alpha)$ and $\delta = (2/3) (1+v^*) (1+\kappa^*) / (1-\alpha)$.

We can next use any five of the six linear equations to solve for B, C and D in terms of A. Given these we can look at equation (B.5) as a non-linear relation between s and θ_1 , which together with equation (B.6) provides a system of two non-linear algebraic equations in s and θ_1 to be solved numerically for a given α (and v). It is observed, however, that equations (B.1) to (B.6) are independent of v for the plane stress case. Hence, for plane stress s , θ_1 and the stress distribution are all independent of v .

Three-region problem ($\alpha^ < \alpha < \alpha^*$).*

Here we have nine unknowns: three real (s , θ_1 , θ_2) and six complex (A, B, C, D, E, F) for a total of fifteen real unknowns. The boundary and continuity conditions include equations (B.1) to (B.4) plus two more equations of the type of (B.3) and (B.4) applied to the reloading boundary ($\theta = \theta_2$). The same unloading condition (B.5) applies, but we must also include a reloading condition which for brevity will not be stated here. In principle, however, given s , θ_1 , θ_2 and (B.1), we can identify a system of ten homogeneous linear equations in the ten unknowns (B, \bar{B} , C, \bar{C} , D, \bar{D} , E, \bar{E} , F, \bar{F}). The zero determinant condition, and the unloading and reloading conditions then provide three non-linear algebraic equations in s , θ_1 and θ_2 which can be solved numerically for given α (and v). Again it is noted that for plane stress s , θ_1 and the stress distributions are independent of v .

Tables

Table 3.1 – Plane stress mode I

α	s(1)	s(2)	s(3)	$\theta_1(1)$	$\theta_1(2)$	$\theta_1(3)$	$\theta_2(1)$	$\theta_2(2)$	$\theta_2(3)$
1.	-0.5	-0.5	-0.5	79.92	79.92	79.92	-	-	-
0.75	-0.469	-0.469	-0.468	81.11	73.10	80.78	-	-	-
0.667	-0.456	-0.456	-0.455	81.58	70.52	80.90	-	-	-
0.5	-0.422	-0.423	-0.420	82.63	64.92	80.76	-	-	-
0.25	-0.340	-	-0.335	84.52	-	78.55	-	-	-
0.1	-0.241	-0.255	-0.237	86.10	46.75	73.65	178.7	-	-
0.01	-0.0896	-0.107	-0.0863	88.28	32.94	61.09	168.8	-	180.0
0.001	-0.0310	-0.0423	-0.0287	89.29	22.61	53.20	160.9	-	180.0
0.0001	-0.0102	-	-0.0093	89.74	-	49.00	156.9	-	180.0

- (1) Deformation theory with unloading condition $\sigma_e'(r, \theta_1-) = 0$
- (2) Deformation theory with unloading condition $\sigma_e'(r, \theta_1+) = 0$
- (3) Flow theory with unloading condition $\sigma_e'(r, \theta_1) = 0$

Table 3.2 – Plane strain mode I ($\nu = 1/3$)

α	s(1)	s(2)	$\theta_1(1)$	$\theta_1(2)$	$\theta_2(1)$	$\theta_2(2)$	$\theta_3(1)$	$\theta_4(1)$
1.	-0.5	-0.5	88.62	88.62	-	-	-	-
0.75	-0.478	-0.478	89.19	91.91	-	-	-	-
0.67	-0.468	-0.469	89.34	93.65	-	-	-	-
0.5	-0.441	-0.442	89.61	98.40	-	-	-	-
0.2	-0.343	-0.300	89.94	113.88	174.8	179.7	-	-
0.1	-0.274	-0.197	89.99	123.35	166.0	173.6	-	-
0.05	-0.269	-0.142	89.99	130.61	139.3	161.0	103.78	137.38
0.04	-0.264	-0.127*	90.00	131.76*	158.2	157.1*	100.93	141.60
0.01	-	-0.0797	-	135.19	-	145.5	-	-

(1) Deformation theory with unloading condition $\sigma_e'(r, \theta_1-) = 0$

(2) Flow theory with unloading condition $\sigma_e'(r, \theta_1) = 0$

(*) Interpolated result

Figures

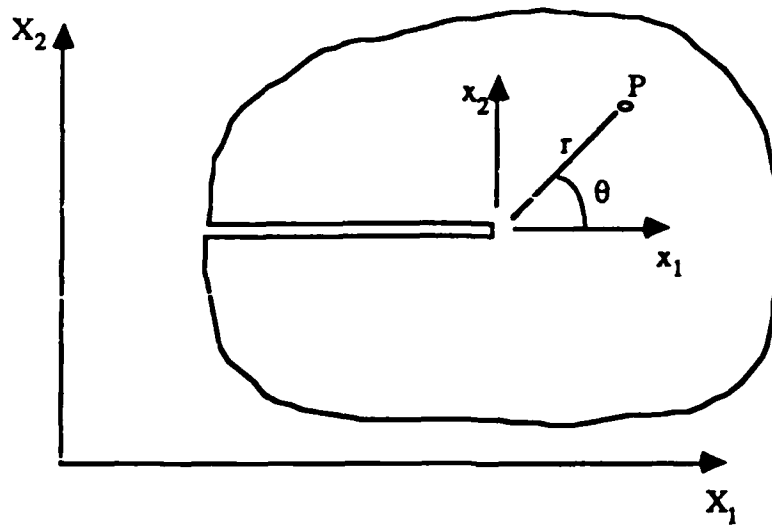


Figure 2.1—Crack-tip geometry

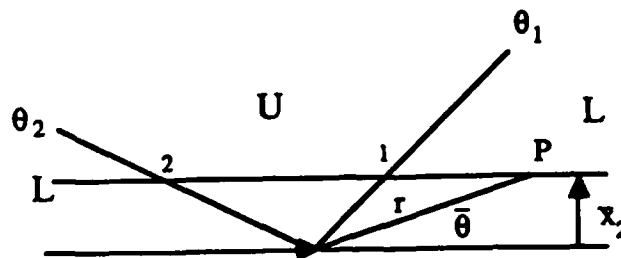


Figure 2.2—Loading history

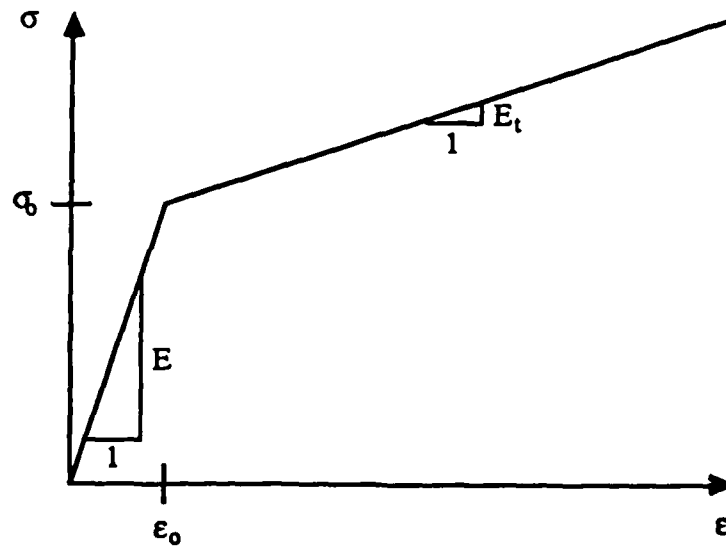


Figure 2.3—Uniaxial stress-strain relation

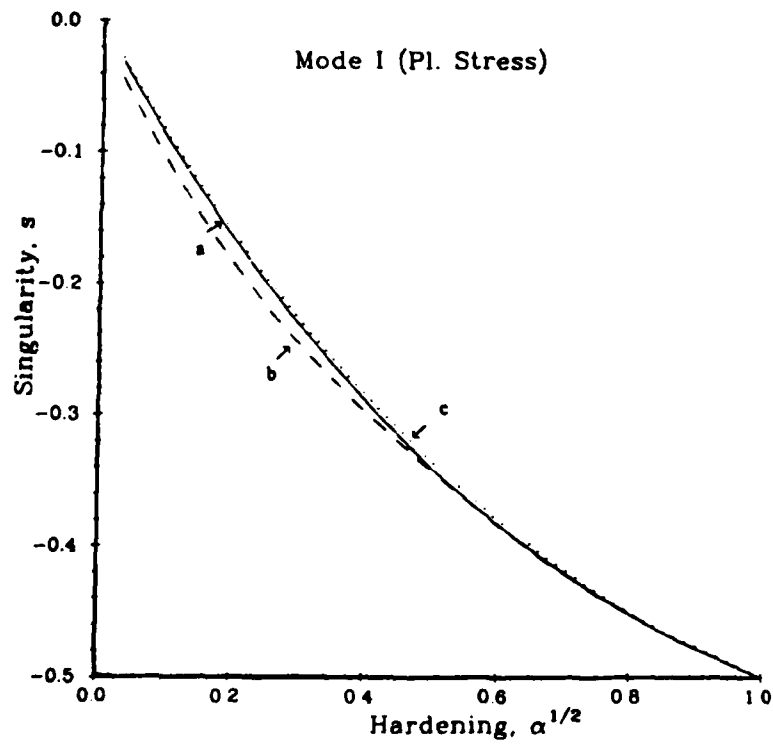


Figure 3.1—Strength of the singularity in plane stress for: (a) deformation theory with unloading condition (2.36a), (b) deformation theory with unloading condition (2.36b), and (c) flow theory.

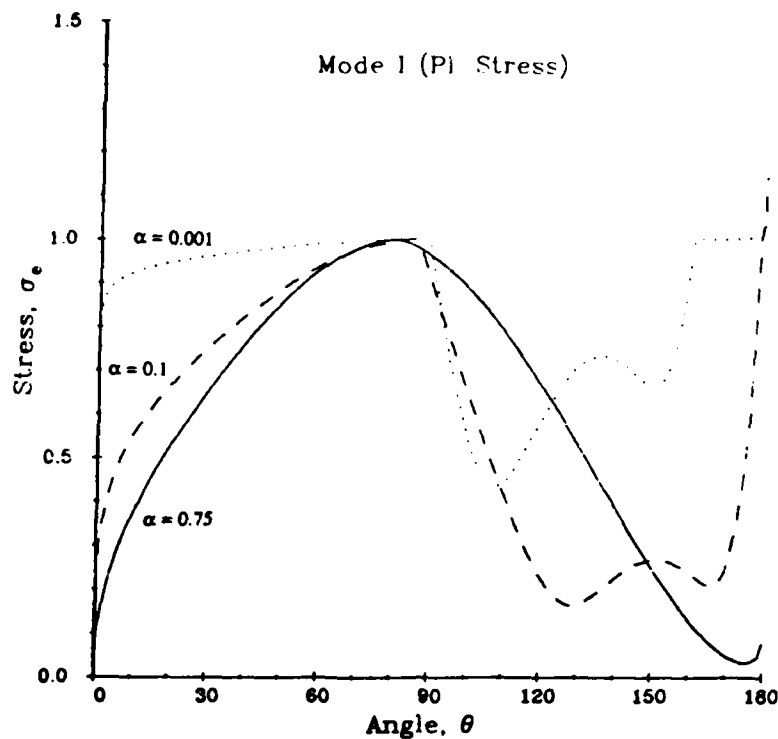


Figure 3.2—Particle (x_2 fixed) effective stress distribution in plane stress for deformation theory with unloading condition (2.36a), normalised such that $\sigma_e(r, \theta_1) = 1$.

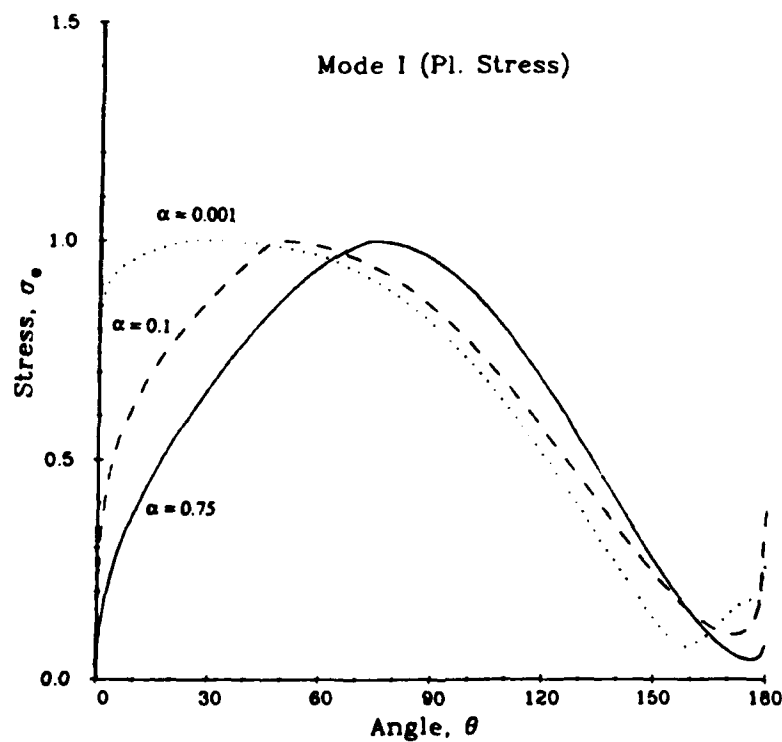


Figure 3.3—Particle (x_2 fixed) effective stress distribution in plane stress for deformation theory with unloading condition (2.36b), normalised such that $\sigma_e(r, \theta_1) = 1$.

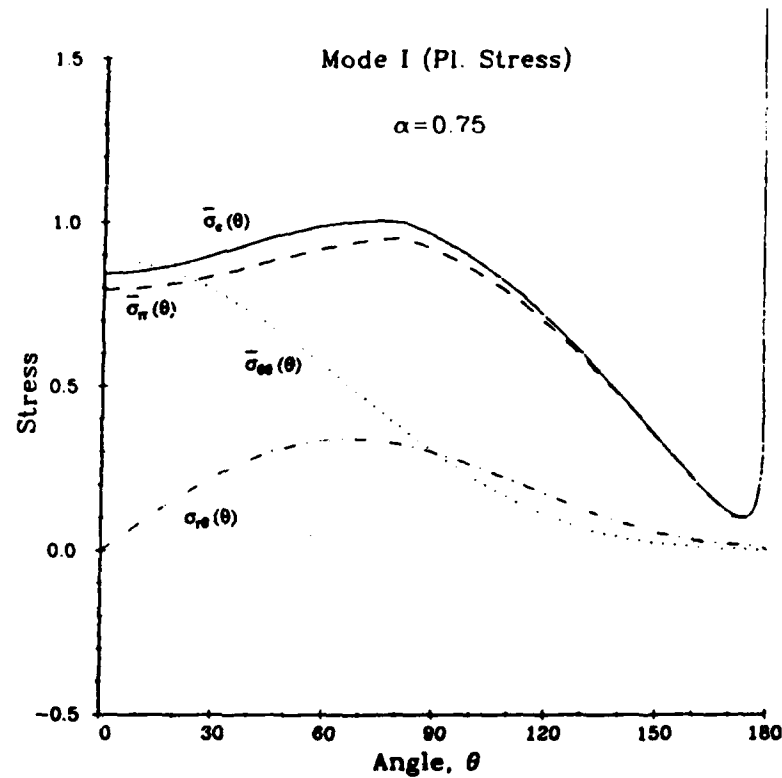


Figure 3.4a—Angular stress distribution in plane stress for deformation theory with unloading condition (2.36a) for large strain-hardening, normalised such that $\bar{\sigma}_r(r, \theta_1) = 1$.

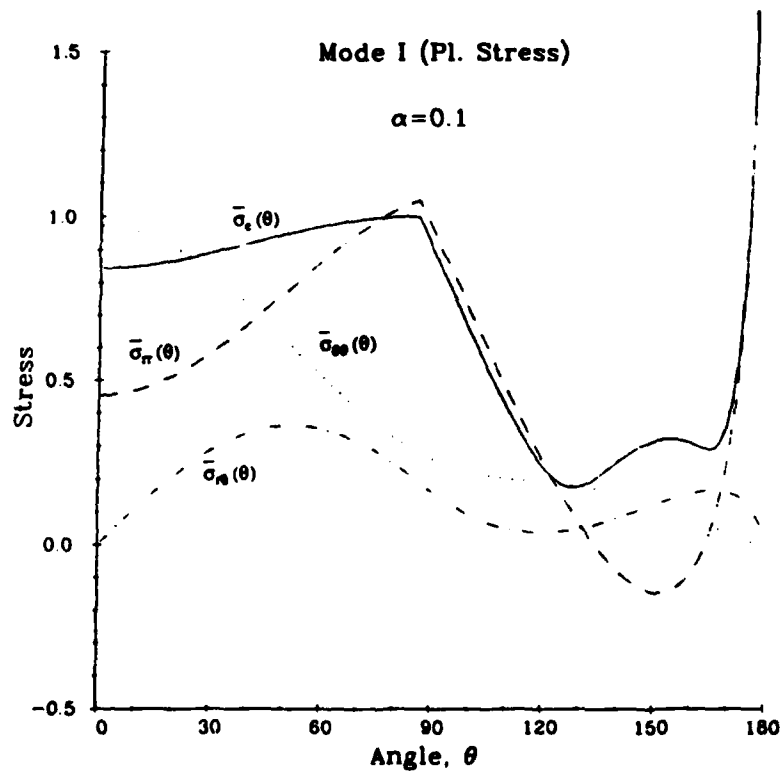


Figure 3.4b—Angular stress distribution in plane stress for deformation theory with unloading condition (2.36a) for moderate hardening, normalised such that $\bar{\sigma}_r(r, \theta_1) = 1$.

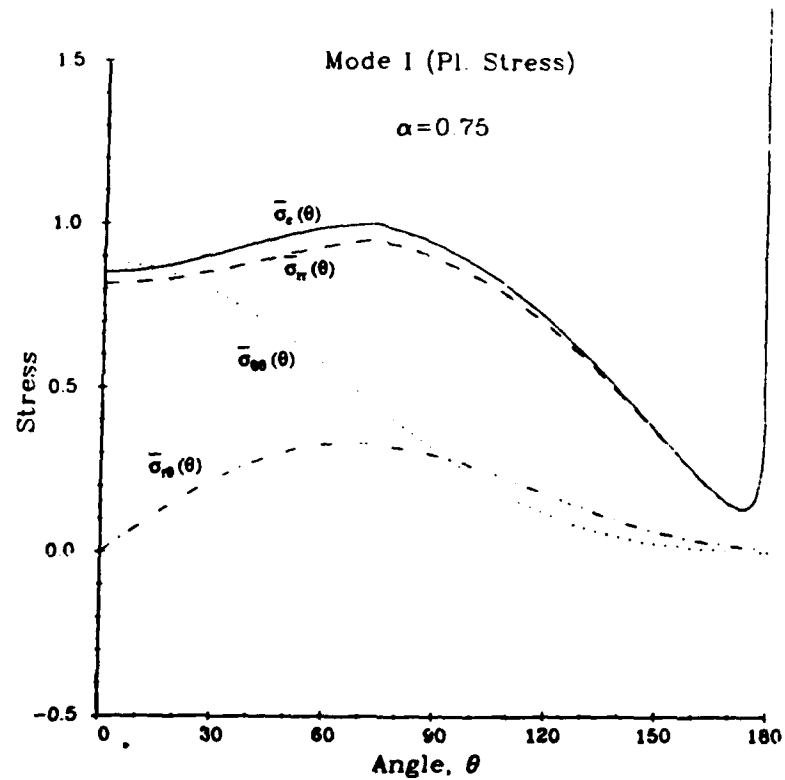


Figure 3.5a—Angular stress distribution in plane stress for deformation theory with unloading condition (2.36b) for large strain-hardening, normalized such that $\bar{\sigma}_e(r, \theta_1) = 1$.

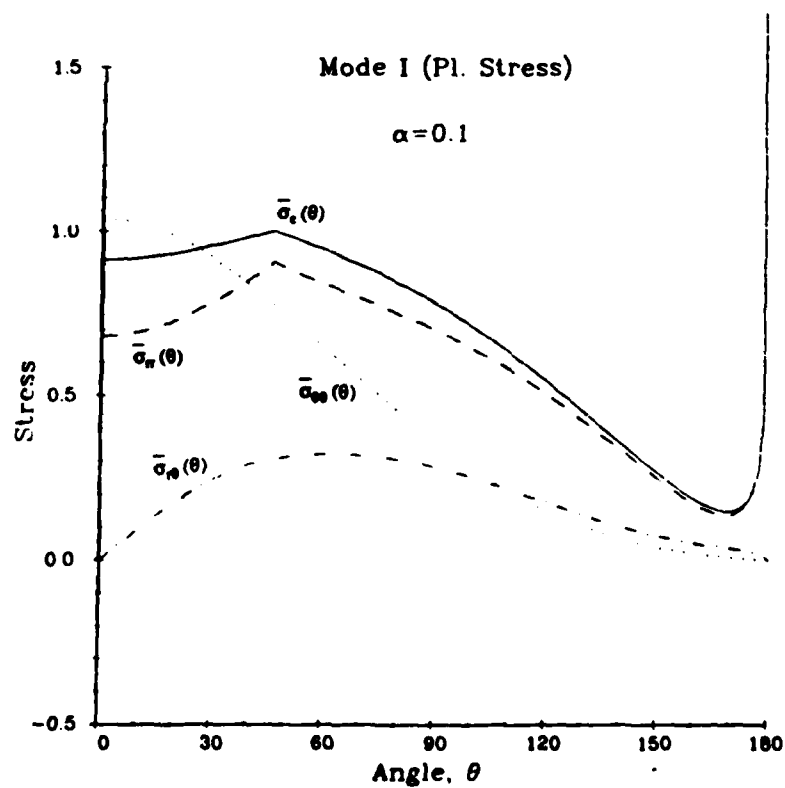


Figure 3.5b—Angular stress distribution in plane stress for deformation theory with unloading condition (2.36b) for moderate hardening, normalized such that $\bar{\sigma}_e(r, \theta_1) = 1$.

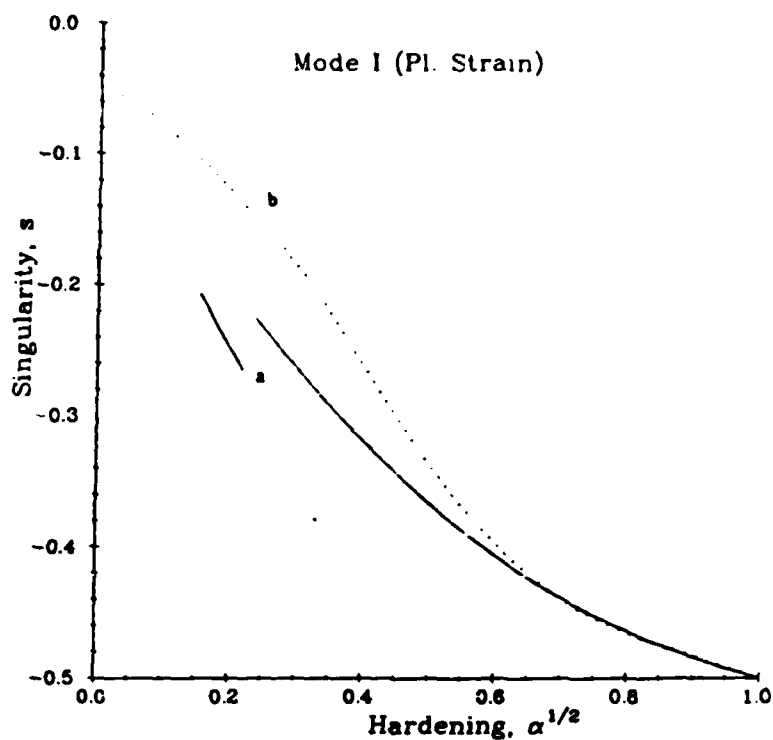


Figure 3.6—Strength of the singularity in plane strain ($\nu = 1/3$) for: (a) deformation theory with unloading condition (2.36a), (b) flow theory.

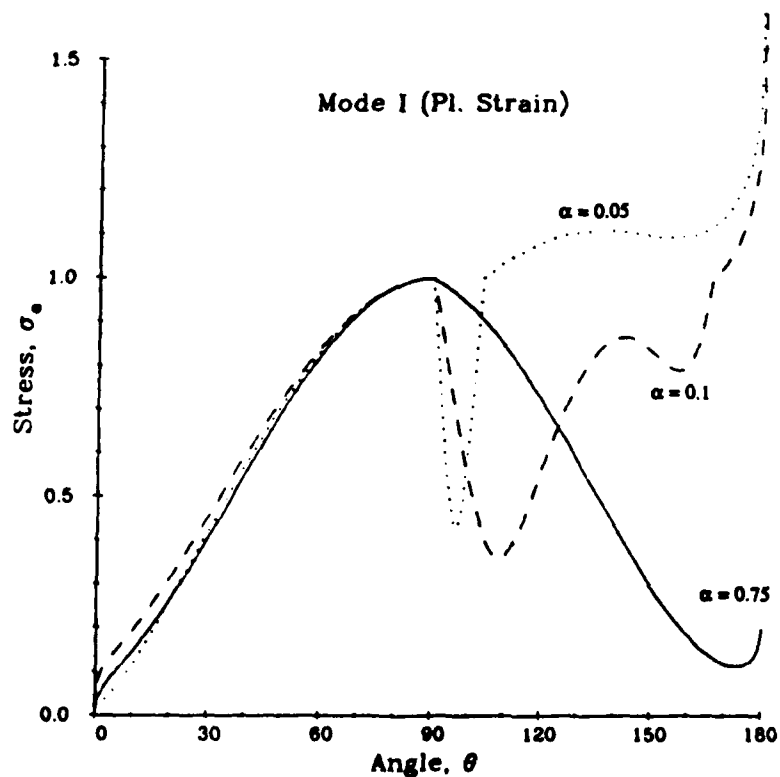


Figure 3.7—Particle effective stress distribution in plane strain ($\nu = 1/3$) for deformation theory with unloading condition (2.36a), normalised such that $\sigma_e(r, \theta_1) = 1$.

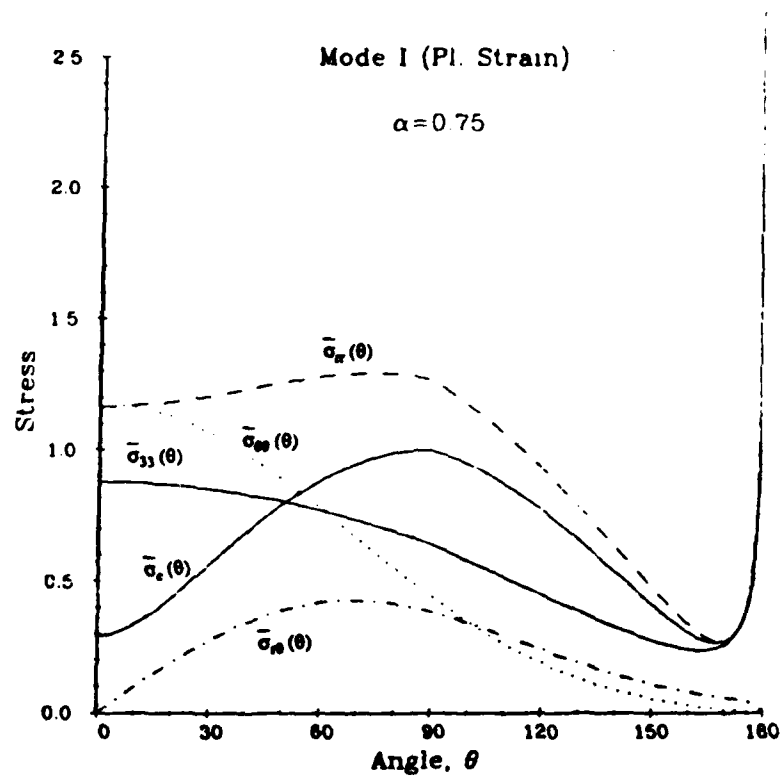


Figure 3.8a—Angular stress distribution in plane strain for deformation theory with unloading condition (2.36a) for large strain-hardening, normalized such that $\bar{\sigma}_e(r, \theta_1) = 1$.

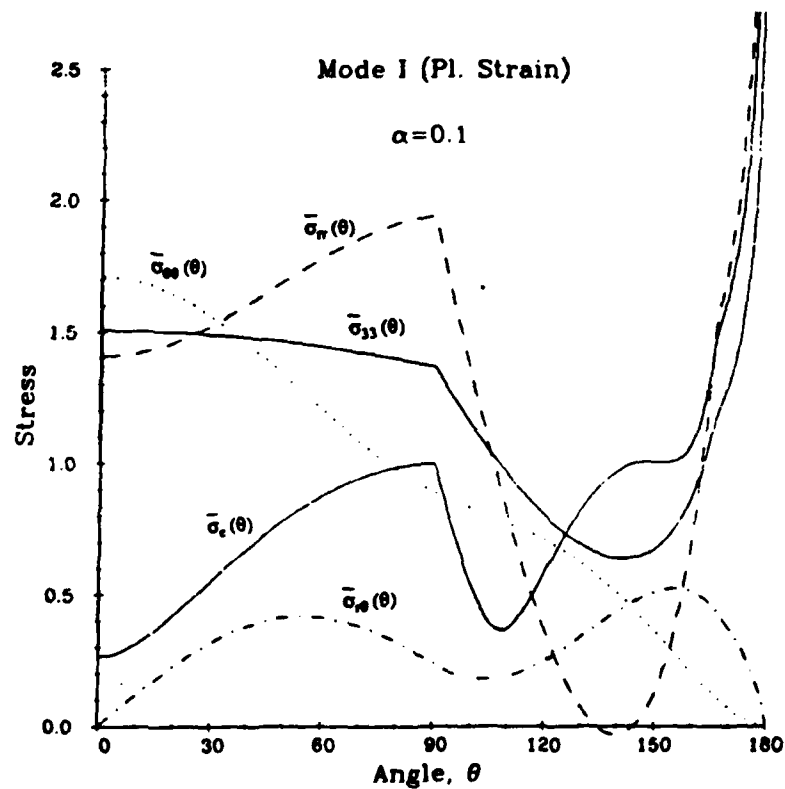


Figure 3.8b—Angular stress distribution in plane strain for deformation theory with unloading condition (2.36a) for moderate hardening, normalized such that $\bar{\sigma}_e(r, \theta_1) = 1$.

END

FILMED

1-86

DTIC